IEEE Access
Multidisciplinary | Rapid Review | Open Access Journal

Date of publication xxxx 00, 0000, date of current version xxxx 00, 0000.

Digital Object Identifier xxx/ACCESS.2021.DOI

A Method for Correcting Frequency Estimates for Synthetic Inertia Control

FELIPE WILCHES-BERNAL[1], (Senior Member, IEEE), JOSH WOLD[2], (Member, IEEE), and W. HILL BALLIET[1], (Member, IEEE)

[1]Sandia National Laboratories, Albuquerque, NM 87185 USA (e-mail: fwilche@sandia.gov)
[2]Montana Technological University, Butte, MT 59701 USA (e-mail: jwold@mtech.edu)

Corresponding author: F. Wilches-Bernal (e-mail: fwilche@sandia.gov).

ABSTRACT This paper presents three frequency estimation algorithms, one based on extended Kalman filtering, another on quadrature phase-locked loop and an adaptive notch filter. The paper proposes using some internal signals of these algorithms as an inverse reliability metric to determine the quality of the frequency estimate. The paper presents an algorithm to correct frequency estimates using these inverse reliability metrics. The algorithm is tested with signals with phase jumps and severe distortions. Accurate frequency estimates are of particular importance in real-time control applications. This paper shows the value of the proposed frequency correction algorithm in synthetic inertia (SI) control. It shows that for a test power system the corrector algorithm is critical in preventing the SI controller from erroneously injecting power that can exacerbate system faults.

INDEX TERMS Adaptive notch filtering, controllable power injections, frequency corrector, frequency estimation, Kalman filter, point-on-wave data, synthetic inertia, low inertia system, phase-locked loop

I. INTRODUCTION

INCREASING penetration of converter interfaced generators (CIGs) is creating unprecedented challenges for inertial response and primary frequency regulation of power systems. This is primarily due to reductions in the amount of available inertia [1], [2]. Enabling CIGs to respond to frequency fluctuations has been identified as a potential solution to the inertia reduction problem [3], [4]. These controllers that help with the inertial response of the system are termed synthetic or virtual inertia controllers and simply intend to emulate the swing equation of conventional generators. In this type of control, the power injection of the CIG is modulated proportionally to the derivative of a frequency estimate (where the frequency estimate plays the role of machine speed for conventional generators). These type of controllers are heavily reliant on accurate frequency estimates which are typically obtained from local voltage measurements.

Frequency estimation of power system signals is a problem that has been constantly studied. A popular family of algorithms for frequency estimation are those based on the discrete Fourier transform (DFT) [5], [6] as these are also the ones typically used by phasor measurement units (PMUs) [7], [8]. Phase-locked loops [9] are another algorithm often used to synchronize power electronic converters to the grid. In addition to those, other estimation algorithms based on Kalman filters [10]–[12], H_∞ filters [13], [14], nonlinear least squares [15], and adaptive notch filters (ANF) have been proposed [16]–[18].

In addition to the issue with inertia reduction, integration of CIGs is affecting the power quality of the system. Lower power quality is reflected in power system signals (voltages and currents) that contain more noise and harmonics and that are prone to heavy distortions when power system disturbances occur. Estimating frequency for these signals is challenging and faulty estimates can lead to faulty decisions. Errors in frequency and rate of change of frequency (ROCOF) estimates have caused false trips in loss of mains relays [19]. The Blue Cut fire event in Southern California where 700 MW of solar power was interrupted was partly due to erroneous frequency estimates of distorted waveforms caused by line-to-line and line-to-ground faults [20]. To prevent such an error from occurring again, NERC recommended delaying protection decisions from frequency measurement. Even though this is a valid solution in certain scenarios it is not an optimal solution in real-time control applications such as synthetic inertia (SI) where the action derived from a frequency measurement is needed almost immediately. Because estimating frequency of heavily distorted signals yields

This article has been accepted for publication in a future issue of this journal, but has not been fully edited. Content may change prior to final publication. Citation information: DOI 10.1109/ACCESS.2020.3044583, IEEE Access

faulty results no matter the algorithm used, recent work has proposed methods to detect distortions or transient events in the input signal and use that information to enhance the frequency estimate. Ref. [21] presents a frequency estimation algorithm that uses a transient detector to inform an *intelligent* frequency estimator to adapt its frequency estimate. In [19] frequency and ROCOF estimates are indirectly corrected by changing the input to the frequency estimation device (in that case a PMU) whenever the input signal is determined to have a phase jump.

A related approach for solving the issue of frequency estimation of distorted signals is to have an estimation algorithm that yields a metric for reliability along with the frequency estimate. The frequency estimate can then be corrected when it is deemed not reliable. This idea was advanced in [10] with a Kalman filter based frequency estimation approach. In that work, the residual of the Kalman filter is used as the inverse reliability metric and a frequency corrector stage was proposed. This paper continues the research in [10] on the use of a frequency correction algorithm to obtain better frequency estimates for distorted signals. In particular, the main contributions of this work are:

- Showing how internal signals of an extended Kalman filter (EKF), quadrature PLL (QPLL), and ANF frequency estimation algorithms can be used as inverse reliability metrics (IRMs) for frequency estimates. The suitability of these signals as IRMs was demonstrated for input signals in the presence of phase jumps and severe distortions. Their performance was also validated under noise conditions.
- Extending the frequency corrector algorithm in [10] by introducing a ramp limit to the frequency corrector. The ramp limit smooths the transition from a corrected value of frequency to a value that is deemed correct. The efficacy of the proposed correction algorithm was demonstrated for the three different estimation algorithm mentioned above.
- Demonstrating the importance of a frequency corrector stage in a SI application. This was done for a power system with a CIG that provides about a quarter of its total load and that has a SI controller enabled. The results presented in this paper show that frequency correction is crucial to prevent a SI controller from affecting the system when a nearby line-to-line or line-to-ground fault occurs.

This paper is organized as follows. Section II presents the fundamentals of frequency estimation in power systems with three different estimation algorithms and proposes an IRM for the frequency estimate. Section III proposes a frequency correction algorithm that uses the IRM. Section IV introduces the test power system used in this work and presents results on the effectiveness of the frequency corrector in a SI application. Finally, Section V presents the concluding remarks and future directions of research for this work.

II. FREQUENCY ESTIMATION IN POWER SYSTEMS

A. SIGNAL MODEL

Typical power system signals can be represented by

$$z(t) = A\cos(\omega t + \phi(t)) \tag{1}$$

where ω is the nominal frequency of the system in rad/s, that is $\omega = 2\pi f_0$, with f_0 as the nominal frequency in Hz. The sampled version of (1) is described by,

$$z_k = A\cos(\omega t_k + \phi(t_k)) \quad k = 1, \ldots, N \tag{2}$$

where $t_k = kT_s$. Relationship (2) can be rewritten, with the help of Euler's formula, as

$$z_k = \frac{A}{2}\left(e^{j(\omega t_k + \phi(t_k))} + e^{-j(\omega t_k + \phi(t_k))}\right) \tag{3}$$

By using the following signals as states

$$x_{1,k} = e^{j\omega T_s} \qquad x_{3,k} = e^{-j\omega T_s} \tag{4}$$

$$x_{2,k} = Ae^{j(\omega k T_s + \phi(t_k))} \qquad x_{4,k} = Ae^{-j(\omega k T_s + \phi(t_k))} \tag{5}$$

a discrete-time state space representation of the sampled sinusoidal waveform in (2) can be found as

$$\mathbf{x}_{k+1} = \begin{bmatrix} x_{1,k+1} \\ x_{2,k+1} \\ x_{3,k+1} \\ x_{4,k+1} \end{bmatrix} = \begin{bmatrix} x_{1,k} \\ x_{2,k} \cdot x_{1,k} \\ x_{3,k} \\ x_{4,k} \cdot x_{3,k} \end{bmatrix} = \mathbf{f}(\mathbf{x}_k) \tag{6}$$

Note that the signal in (3) can be obtained from the states in (6) as

$$z_k = \begin{bmatrix} 0 & \frac{1}{2} & 0 & \frac{1}{2} \end{bmatrix} \mathbf{x}_k \tag{7}$$

B. EXTENDED KALMAN FILTER

The Kalman Filter is an estimation technique widely used for tracking and data prediction. It was initially proposed in 1960 for linear systems [22]. Since then a series of developments have allowed it to be used in nonlinear systems. This paper uses the Extended Kalman Filter (EKF) used in [10]–[12] for frequency estimation. Due to space limitations other techniques like the Unscented Kalman Filter (UKF) were evaluated but not included here. The EKF is used for a system of the form

$$\mathbf{x}_{k+1} = \mathbf{f}(\mathbf{x}_k) + \mathbf{w}_k \tag{8}$$

$$\mathbf{z}_k = \mathbf{h}(\mathbf{x}_k) + \nu_k \tag{9}$$

where (8) and (9) are, respectively, the system and measurement equations. $\mathbf{x}_k \in \mathbb{R}^n$ and $\mathbf{z_k} \in \mathbb{R}^m$ are the system and measurement state vectors at the k^{th} step, respectively. The process noise $\mathbf{w}_k$ and the measurement noise $\nu_k \in \mathbb{R}^m$ are described by

$$E[w_k] = 0 \quad E[w_k w_k^\top] = \mathbf{Q}_k \quad E[w_k w_j^\top] = 0 \text{ for } k \neq j \tag{10}$$

$$E[v_k] = 0 \quad E[v_k v_k^\top] = \mathbf{R}_k \quad E[v_k v_j^\top] = 0 \text{ for } k \neq j \tag{11}$$

$$E[w_k v_j^\top] = 0 \text{ for all } k \text{ for all } j \tag{12}$$

$$\mathbf{Q}_k = \mathbf{Q} \text{ and } \mathbf{R}_k = \mathbf{R} \; \forall \; k \tag{13}$$

This article has been accepted for publication in a future issue of this journal, but has not been fully edited. Content may change prior to final publication. Citation information: DOI 10.1109/ACCESS.2020.3044583, IEEE Access

Algorithm 1 Extended Kalman Filter

Time Update (or Predictor Update)

1. Predict the state:

$$\hat{\mathbf{x}}_k^- = \mathbf{f}(\hat{\mathbf{x}}_{k-1})$$

2. Linearize the system:

$$\mathbf{F}_{k-1} = \left.\frac{\partial \mathbf{f}(\mathbf{x})}{\partial \mathbf{x}}\right|_{\mathbf{x}=\hat{\mathbf{x}}_{k-1}}$$

3. Predict the covariance:

$$\mathbf{P}_k^- = \mathbf{F}_{k-1}\mathbf{P}_{k-1}\mathbf{F}_{k-1}^\top + \mathbf{Q}$$

Measurement update (or filter update)

4. Linearize the measurement:

$$\mathbf{H}_k = \left.\frac{\partial \mathbf{h}_k(\mathbf{x})}{\partial \mathbf{x}}\right|_{\mathbf{x}=\hat{\mathbf{x}}_k^-}$$

5. Measurement residual:

$$\mathbf{e}_k = \mathbf{z}_k - \mathbf{h}(\hat{\mathbf{x}}_k^-)$$

6. Measurement covariance:

$$\mathbf{S}_k = \mathbf{H}_k\mathbf{P}_k^-\mathbf{H}_k^\top + \mathbf{R}$$

7. Compute the Kalman Gain:

$$\mathbf{K}_k = \mathbf{P}_k^-\mathbf{H}_k^\top\mathbf{S}_k^{-1}$$

8. Update the state:

$$\hat{\mathbf{x}}_k = \hat{\mathbf{x}}_k^- + \mathbf{K}_k\mathbf{e}_k$$

9. Update the covariance:

$$\mathbf{P}_k = (\mathbf{I} - \mathbf{K}_k\mathbf{H}_k)\mathbf{P}_k^-$$

Algorithm 1 presents the step-by-step EKF procedure.

The EKF frequency estimator tracks a sinusoidal waveform with a certain amplitude, frequency and phase. The information on frequency is in states $x_{1,k}$ and $x_{3,k}$. The frequency estimate, $\hat{f}_k$, can be obtained from these states as[1]

$$\hat{f}_k = \frac{f_s}{2\pi}\cos^{-1}\left(\frac{x_{1,k}+x_{3,k}}{2}\right) \tag{14}$$

where $f_s = 1/T_s$ is the sampling frequency. The magnitude of the residual can be used as an IRM for the frequency estimate. That is,

$$r_k = |\mathbf{e}_k|$$

where r_k represents the IRM at time step k.

C. QUADRATURE PLL

The quadrature phased-locked loop (QPLL) is a control system similar to the traditional PLL but that differs from it in the mechanism for phase detection. The QPLL is an effective mechanism for frequency estimation. The structure of the QPLL used in this work is presented in [23] and is described by

$$\frac{dk_s(t)}{dt} = \dot{k}_s(t) = 2\mu_s e(t)\sin(\phi(t)) \tag{15}$$

$$\frac{dk_c(t)}{dt} = \dot{k}_c(t) = 2\mu_c e(t)\cos(\phi(t)) \tag{16}$$

$$\frac{\Delta\omega(t)}{dt} = \Delta\dot{\omega}(t) = 2\mu_f e(t)\left[k_s\cos(\phi(t)) - k_c\sin(\phi(t))\right] \tag{17}$$

$$\frac{d\phi(t)}{dt} = \dot{\phi}(t) = \Delta\omega(t) + \omega_0 \tag{18}$$

$$y(t) = k_s\sin(\phi(t)) + k_c\cos(\phi(t)) \tag{19}$$

$$e(t) = z(t) - y(t) \tag{20}$$

The block diagram of the QPLL is presented in Fig. 1. Note that $z(t)$ in (20) is the signal defined in (1).

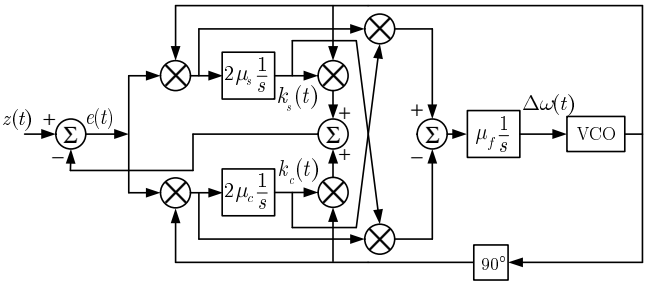

FIGURE 1. Block diagram of the QPLL.

For the QPLL algorithm a valid IRM is

$$r(t) = \left|\frac{\mathrm{d}}{\mathrm{d}t}\sqrt{k_s^2(t)+k_c^2(t)}\right| \tag{21}$$

The value in $\sqrt{k_s^2(t)+k_c^2(t)}$ is the estimated amplitude of the signal which is constant for clean sinusoidals. In contrast, every time distortion is present in the input signal the amplitude presents an erratic behavior. The derivative of this value is then higher for signals with distortion and close to zero for those without it. This derivative is the value presented in (21). It is important to note that the intrinsic error function in (19) is not suitable as an IRM because it has an oscillatory behavior in steady state. For further information on this frequency estimation technique, the interested reader is referred to [23] .

D. ADAPTIVE NOTCH FILTER

Another frequency estimation algorithm is the ANF [16]–[18]. Notch filters are band-stop filters that ideally only stop one frequency: the so-called notch frequency. Notch filters can then estimate the frequency of a given sinusoidal input provided it remains constant. The ANF is able to track changes in freuqency of an input signal by simply adjusting its notch frequency. Several ANF structures have been

[1] An alternative approach to compute the frequency is: $f_k = \frac{f_s}{2\pi}\left|\mathrm{Im}\left[\log(x_{1,k})\right]\right|$

proposed. The particular ANF structure used in this work is defined by the following differential equations ANF [17]

$$\frac{d\nu_1}{dt} = \dot{\nu}_1 = \nu_2 \tag{22}$$

$$\frac{d\nu_2}{dt} = \dot{\nu}_2 = 2\zeta(z - \nu_2)\nu_3 - \nu_1\nu_3^2 \tag{23}$$

$$\frac{d\nu_3}{dt} = \dot{\nu}_3 = -\gamma_I(z - \nu_2)\nu_1\nu_3 \tag{24}$$

where ν_3 is the estimated frequency of the input signal $z(t)$ (as defined in (1)). The ANF above has 3 states: ν_1, ν_2, ν_3 and one input z. The error signal of the ANF can be expressed as

$$e(t) = r(t) = |z(t) - \nu_2(t)| \tag{25}$$

and can be used as an IRM for the frequency estimate.

III. FREQUENCY CORRECTION

A. INVERSE RELIABILITY METRICS

This section shows how the IRMs of the three frequency estimation algorithms outlined in Section II are affected by distortions (or disturbances) of the input signal.

Fig. 2 shows a sinusoidal waveform with a phase step of -40° occurring at approximately 6 seconds. Fig. 3 shows how the IRM of the EKF, QPLL, and ANF respond to the phase step. Because these IRMs come from different frequency estimation algorithms they are generally not at the same scale; hence, the results in Fig. 3 show a normalized version. That is, the maximum value for each IRM was set to 1. The normalization allows comparison of the different IRMs. The results in Fig. 3 show that the IRM for all estimation algorithms responds similarly following the event. In particular this figure shows: (i) for all cases the IRM reaches its maximum value immediately after the distortion; (ii) before the event the metric is almost zero for all cases and it returns to zero after about 0.18 seconds; (ii) following the event the IRM has a decaying oscillatory behavior with a frequency of ∼120 Hz in the case of the EKF and ANF and almost twice that value in the case of the QPLL.

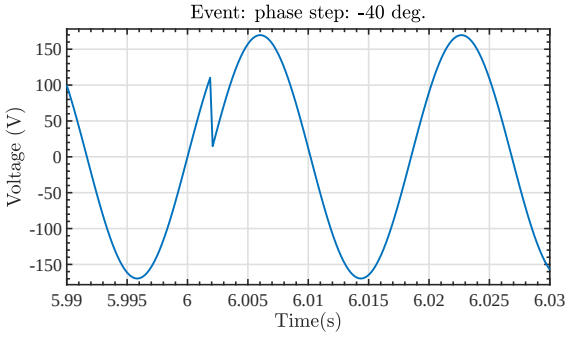

FIGURE 2. Sinusoidal waveform with a phase step of -40°.

Fig. 4 shows the estimated frequency obtained with the EKF, QPLL, and ANF methods for the signal with the phase step in Fig. 2. For comparison, this figure also shows the

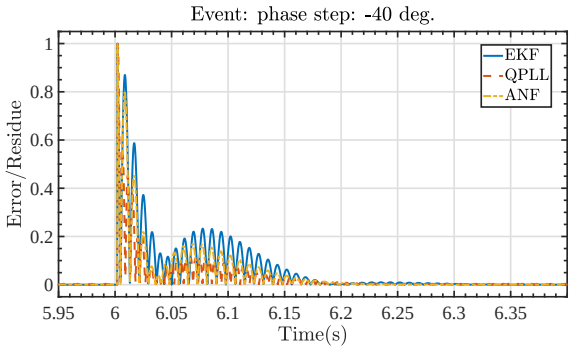

FIGURE 3. IRM of the EKF, QPLL, and ANF frequency estimation algorithms for the signal with the phase step in Fig. 2.

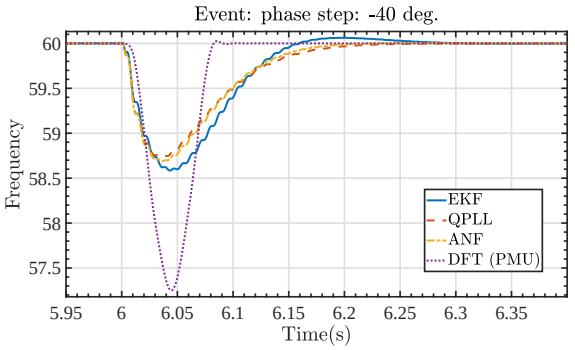

FIGURE 4. Estimated frequency with the EKF, QPLL, and ANF for the signal in Fig. 2.

estimated frequency with a DFT based method (the specific configuration used has the same structure as the one recommended in [8] for PMUs but some differences in the filtering). The figure shows that the phase step distortion causes a drop in the estimated frequency for all the methods under consideration. In particular, the three estimation algorithms presented in Section II produce very similar frequency estimates with a drop of around 1.5 Hz while the drop experienced by the frequency estimate of the PMU-like algorithm is higher and reaches about 2.9 Hz. This deviation in frequency lasts for about 0.2 for the EKF, QPLL, and ANF and only 0.1 Hz for the DFT estimation method. We note the responses observed by the EKF, QPLL, and ANF algorithms are dependent on the specific parameter of each method.

Fig. 5 shows the IRM of the EKF, QPLL, and ANF when the input signal in Fig. 2 has a signal to noise ratio (SNR) of 40 dB. This noise level was selected because it has been reported this is a conservative for typical point-on-wave data. This result was also verified experimentally with actual recordings from digital fault recorders (DFRs). The results are normalized just as those in Fig. 3 when the signal has no noise. These results show that the noise does not significantly affect how the IRM respond to the severe distortion. The primary difference is that in steady-state instead of being almost zero the IRM has an average value of 0.009 with frequency maximum values around 0.05.

This article has been accepted for publication in a future issue of this journal, but has not been fully edited. Content may change prior to final publication. Citation information: DOI 10.1109/ACCESS.2020.3044583, IEEE Access

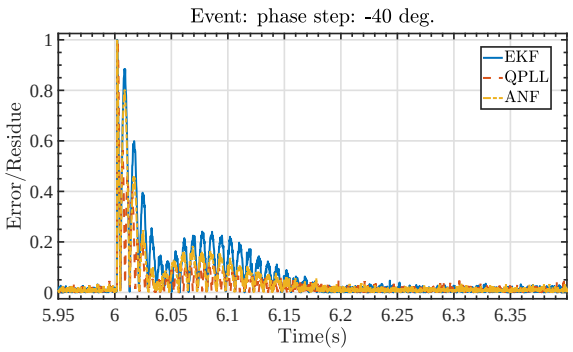

FIGURE 5. IRM of the EKF, QPLL, and ANF frequency estimation algorithms for the signal with the phase step in Fig. 2 with an SNR of 40dB.

B. CORRECTION ALGORITHM

Frequency estimation from signals that can be accurately described by (1) is a relatively simple procedure. Frequency can be successfully estimated by several techniques such as those presented in Section II. However, for signals that are not accurately represented by (1), frequency estimation may pose challenges. This is particularly true for signals that are not periodic and for which the very definition of frequency is an *open question*. In power systems, severely distorted signals for short time intervals are common at nearby buses following system disturbances such as line-to-line or three-phase faults. Estimating the frequency from those signals yields defective results regardless of the estimation technique utilized. However, as we have seen in Section III-A whenever there is a severe distortion and the frequency estimate is most likely erroneous, the IRM increases. The estimation algorithms used in this work can be thought as systems that have two outputs: a frequency estimate $f(t)$ (or $\hat{f}_k$ in discrete time) and IRM $r(t)$ ($\hat{r}_k$ in discrete time). This concept is observed in Fig. 6.

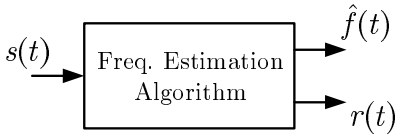

FIGURE 6. Schematic of frequency estimation.

Because the IRM increases whenever there is a distortion and the frequency estimate is likely faulty, it can be used as a flag to mark these estimates and correct them. The idea of correcting frequency estimates using a IRM has been introduced in [10] for the KF frequency estimation algorithm used in this paper. The solution consists of *correcting* the frequency estimate when the magnitude of the IRM (r_k) surpasses a user-defined threshold (ϵ). When this condition is met the frequency estimate is deemed incorrect and the corrected frequency is held to a previous value. This hold value is returned to the estimated value by the estimation algorithm only after r_k has been below the threshold ϵ for a certain user-defined period of time t_{hold}. This paper extends the frequency corrector algorithm described above, and presented in [10], to incorporate a rate limiter for the corrected frequency. The rate limiter (R_{fmax}) is enabled only after the frequency estimate is considered reliable again and a transition needs to be made between the value at which the corrector holds the frequency and the current frequency estimate. The purpose of the rate limiter is to avoid undesirable jumps in the output of the frequency corrector. For control applications, avoiding jumps in the estimated frequency will help produce a smoother (or bumpless) control signal. This procedure, including the rate limiter extension, is presented in Algorithm 2. Note that in this algorithm, $\hat{f}_k$ is the input and $\hat{f}_k^{\text{corr}}$ is the output. F_{tH} is a binary variable that indicates that the IRM has surpassed the threshold (ϵ) and the frequency should be held at a safe value $\hat{f}_{\text{prev}}$. F_{tH} is active whenever ϵ is larger than the limit and for t_{hold} after it goes below the threshold. Similarly, F_{ramp} is a binary variable that determines when the rate limiter is active after the action of holding the frequency, determined by F_{tH}, has subsided.

Algorithm 2 Frequency Correction Algorithm

if ($|r_k| < \epsilon$ **and** $\neg F_{\text{tH}}$ **and** $\neg F_{\text{ramp}}$) **then**
  $\hat{f}_k^{\text{corr}} \leftarrow \hat{f}_k$
else if $|r_k| < \epsilon$ **and** F_{tH} **and** F_{ramp} **then**
  if $t_{\text{cont,k}} > t_{\text{hold}}$ **then**
    $F_{\text{tH}} \leftarrow$ False
  end if
  $\hat{f}_k^{\text{corr}} \leftarrow \hat{f}_{\text{prev}}$
  $t_{\text{cont,k}} = t_{\text{cont,k}-1} + T_s$
else if $|r_k| < \epsilon$ **and** $\neg F_{\text{tH}}$ **and** F_{ramp} **then**
  $\Delta\hat{f}_k = \hat{f}_k - \hat{f}_{k-1}^{\text{corr}}$
  if $|\Delta\hat{f}_k| > R_{\text{fmax}}$ **then**
    $\Delta\hat{f}_k \leftarrow \text{sgn}(\Delta\hat{f}_k) R_{\text{fmax}}$
  else
    $F_{\text{ramp}} \leftarrow$ False
  end if
  $\hat{f}_k^{\text{corr}} \leftarrow \hat{f}_{k-1}^{\text{corr}} + \Delta\hat{f}_k$
else if $|r_k| > \epsilon$ **then**
  $\hat{f}_k^{\text{corr}} = \hat{f}_{\text{prev}}$
  Reset time: $t_{\text{cont,k}} \leftarrow 0$
  $F_{\text{tH}} \leftarrow$ True
  $F_{\text{ramp}} \leftarrow$ True
end if

The three estimation algorithms used in this work are control systems that produce frequency estimates continuously as they receive input data. These frequency estimates are continuously adapted so that the difference between the measurement and a signal estimate is minimized. These methods produce signals that can be used as IRMs as presented above. A window-based estimation algorithm such as nonlinear least squares can also produce a similar metric. Yet another family of algorithms such as those used by PMUs do not have an explicit metric. However, with such an approach, based on the estimates (amplitude, phase and frequency) an ideal signal

This article has been accepted for publication in a future issue of this journal, but has not been fully edited. Content may change prior to final publication. Citation information: DOI 10.1109/ACCESS.2020.3044583, IEEE Access

can be reconstructed and compared with the measurement. From this comparison a metric for reliability (and its inverse) can be proposed [24].

Corrected frequency estimates (and their associated ROCOF) are instrumental in power system monitoring and control applications which require extremely accurate measurements even in situations where the signal is distorted. The algorithm presented here is useful in such cases. An alternative for correcting frequency measurement has been presented in [19]. In that case, whenever a phase step is detected in the input signal, it is replaced with a cleaner reconstruction of it. This method was proposed for a PMU estimator.

C. FREQUENCY CORRECTION EXAMPLES

This section shows examples of using Algorithm 2 to correct frequency estimates.

Fig. 7 shows the frequency estimates obtained with the three estimation algorithm in Section II in addition to the DFT method recommended for PMUs for the signal in Fig. 2 with a 40 dB SNR. In addition to the frequency estimates obtained from the three algorithms, the corrected values for those using Algorithm 2 are also shown. The results in Fig. 7 show that the proposed frequency correction technique is able to suppress the frequency drop. In this example the estimate was held at the nominal value, 60 Hz, which is the level before the IRM flags the estimate as incorrect.

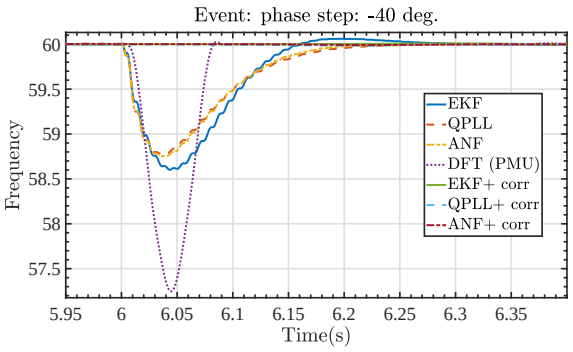

FIGURE 7. Estimated frequency with the EKF, QPLL, ANF and DFT for the signal in Fig. 2 with a 40dB SNR. Corrected frequency estimates are also shown in this figure.

Fig. 8 shows the same information as Fig. 7 but the y-axis is zoomed in around the nominal frequency to highlight the effect of the frequency corrector. The results in this figure show that following the phase step in the signal, the frequency corrector holds the frequency to a correct value and for a short period of time. The value at which the frequency is held, as well as the duration of this action are different for the three estimation algorithms but very close to the nominal value. Fig. 8 also shows the effect of the rate limiter on the frequency estimates. The frequency estimate for all the algorithms under consideration behaves as a straight line with a slope when transitioning from the held value to a new correct one.

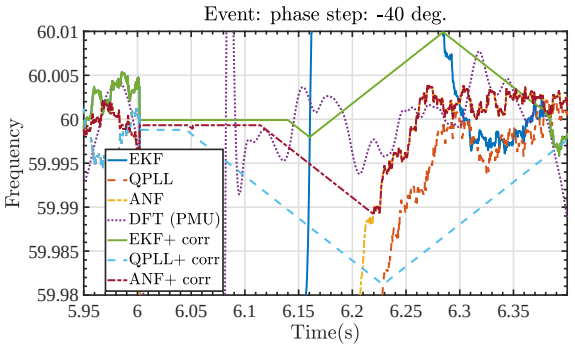

FIGURE 8. Estimated frequency with the EKF, QPLL, ANF and DFT for the signal in Fig. 2 with a 40dB SNR. Corrected frequency estimates are also shown in this figure. The y-axis has been zoomed in around the nominal frequency to show the effect of the frequency corrector.

Fig. 9 shows the phase A voltage signal at a location that is electrically close to a line-to-line fault that occurs at 5 seconds. The fault is cleared 50ms later but that cannot be observed in the figure. In this signal, it is observed that the fault causes both the phase and amplitude of the signal to abruptly change. Estimating frequency for those types of signals is often difficult; in fact, similar signals were partially responsible for the 2016 Blue Cut fire event in Southern California [20].

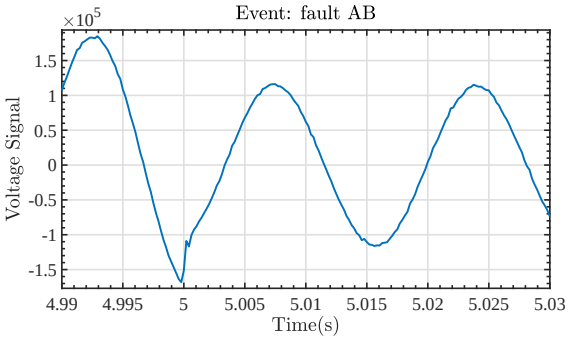

FIGURE 9. Voltage waveform of a line-to-line fault.

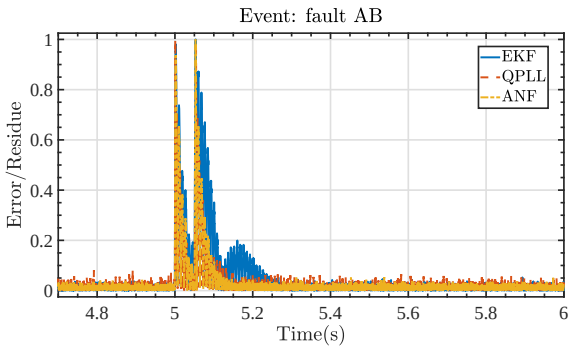

FIGURE 10. IRM of the EKF, QPLL, and ANF methods for the the signal in Fig. 9.

Fig. 10 shows the normalized IRM of the EKF, QPLL, and ANF for the signal in Fig. 9 with added noise for a

This article has been accepted for publication in a future issue of this journal, but has not been fully edited. Content may change prior to final publication. Citation information: DOI 10.1109/ACCESS.2020.3044583, IEEE Access

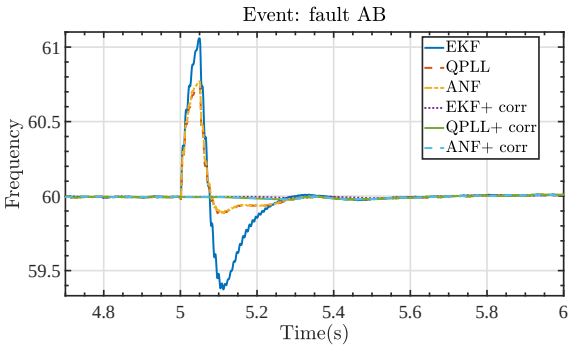

FIGURE 11. Estimated frequency with the EKF, QPLL, and ANF, and their associated corrected estimates for the signal in Fig. 9.

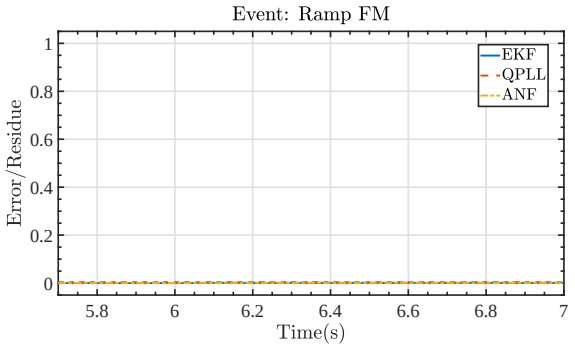

FIGURE 12. IRM of the EKF, QPLL, and ANF methods for a signal experiencing a frequency ramp starting at 6 s with a slope of -0.1 Hz. The IRM was normalized with the same values as those in Fig 3.

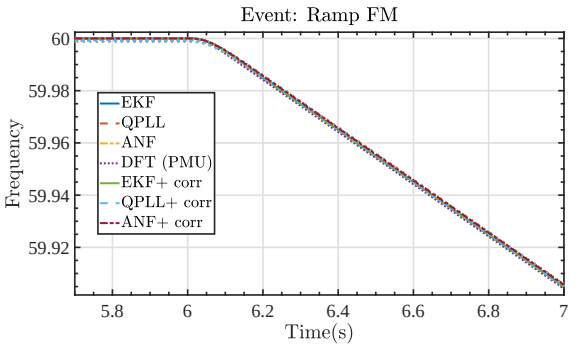

FIGURE 13. Estimated frequency with the EKF, QPLL, ANF and DFT for the signal with the frequency ramp starting at 6 s with a slope of -0.1 Hz.

SNR of 40dB. The results in this figure show that the IRM spikes when the fault occurs and when the fault is cleared but decays in between those two events. It can also be observed that the IRM associated with the EKF exhibits higher values that those associated with the other algorithms after the fault is cleared. Fig. 11 shows the frequency estimates and their associated corrected values for the EKF, QPLL, and ANF. These results show that the distortion to the voltage waveform caused the frequency estimate to take initially positive values reaching around 61 Hz, 50 ms after the fault for all the estimation algorithms. After this maximum value is reached, the estimate starts decreasing until it crosses the nominal value around 85 ms after the event. At that point the EKF frequency estimate keeps decreasing until 59.4Hz while the estimates for the QPLL and the ANF only reach 59.86 Hz. The results in Fig. 11 also show the corrected values when Algorithm 2 is applied; in those cases the frequency does not experience any significant deviation from its steady-state value (note that in steady state the estimate is not constant but instead it exhibits small variations around the nominal value which can be attributed to the noise added to the signal).

For completeness, this paper also presents the behavior of the frequency corrector for a signal experiencing a modulation in frequency in the form of a ramp. The modulation starts at 6 seconds with rate of change of -0.1Hz/s. Fig. 12 shows the normalized IRM of the EKF, QPLL, and ANF algorithms for this signal. Note that the values presented in this figure were normalized, per algorithm, with the same constant as those in Fig 3. This is because the IRM for this type of disturbance to the signal never has a significant value (for either algorithm) and normalization in such scenario is not helpful. Normalizing the IRM for this signal with the values obtained for the phase step shows that in a case of a smooth (*and real*) frequency change the proposed IRM is not harmful to the frequency estimation process. Fig. 13 shows the frequency estimates for all the estimation methods for the frequency ramp case. The figure shows that the results with the corrector are the same as those without it. This was expected because as mentioned above, the IRMs are always low.

It is important to note to the user that in practice the IRMs are not normalized. This was done in the paper so that a comparison could be made across algorithms. In practice what should be done is to determine what the IRM value is for a severe event such as a phase step, and what it is for a smooth change such as a ramp modulation. These values should vary significantly and ϵ of Algorithm 2 can be set to a value in between them.

IV. FREQUENCY CORRECTION IN SYNTHETIC INERTIA CONTROL

A. POWER SYSTEM MODEL

This paper uses the system in Fig. 14 to test the efficacy of the proposed frequency corrector in SI control. The system is a modified version of the well-known KRK 2-Area system in [25] and has 6 generators. G1 and G2, in Area 1, each have a rating of 1000 MW. G3 in Area 2 has a rating of 900 MW. Generators G4, G5, and G6, also in Area 2, have, respectively, machine ratings of 450, 225, and 225 MW. The operating condition for the system used in this work has G1, G2 and G3 with a power level of 700MW while G4, G5, and G6, respectively, produce 450, 225 and 225 MW. Load LA1 in Area 1 and LA2 in Area 2 consume 950 and 1540MW, respectively. Note that G2 is the swing bus and its actual power is adjusted during the loadflow computation. This system was implemented in Simscape from Matlab/Simulink [26].

This research considers the following cases to study the effect of different implementations of SI control in the system:

This article has been accepted for publication in a future issue of this journal, but has not been fully edited. Content may change prior to final publication. Citation information: DOI 10.1109/ACCESS.2020.3044583, IEEE Access

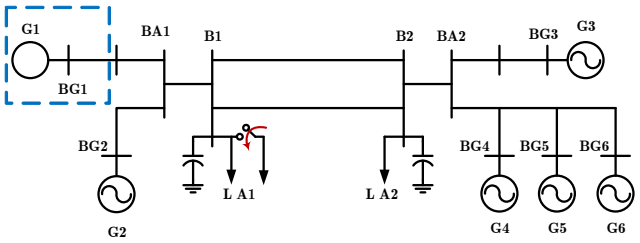

FIGURE 14. Test power system used in this work: a modified version of the 2-area KRK system.

- the base case with the system as described above;
- the 25% no control case where G1 is fully replaced by a CIG that is not responsive to frequency deviations;
- the case where G1 is replaced by CIG that has the SI controller in Section IV-B without using the frequency correction algorithm;
- the same configuration as above but with the correction algorithm active.

B. SYNTHETIC INERTIA CONTROL

This paper uses the SI controller presented in Fig. 15. This type of controller tries to imitate the inertial response of synchronous generator by modulating the active power of the CIG with the derivative of a frequency measurement. This frequency measurement plays the role the speed has in a synchronous machine and it was selected to be the frequency estimate of the local voltage measurements. The frequency estimation algorithm selected for the results of this paper was the EKF (but similar results are obtained with the QPLL and ANF). An important difference between the controller in Fig. 15 and a typical SI controller is the presence of the frequency correction stage. This stage was made optional in order to show the benefits of including it. The corrector stage is based on Algorithm 2. The input signal is the local voltage where the CIG is included. The values for the parameters of the frequency corrector are: $\epsilon = 0.05$, $t_{hold} = 20$ ms, $R_{fmax} = 20\ \mu s^{-2}$. We also note that for a SI to be stable a filtering stage is needed. Intuitively, this is because the presence of the derivative in a SI controller needs to be compensated at some frequency. The details of the filter design are beyond the scope of this paper but the interested reader is referred to [26].

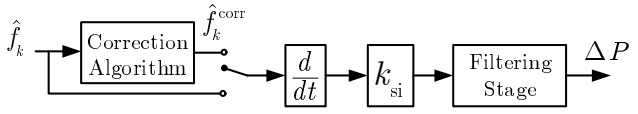

FIGURE 15. SI controller that includes the frequency corrector used in this paper.

C. RESULTS FOR POWER SYSTEM DISTURBANCES

In addition to the SI control cases detailed in Section IV-A, this research considers three different power system disturbances:

- Connecting a load of 150 MW in Area 1 at 2.5 seconds. This case is selected to show that the SI controller used in this work is effective in mitigating the effects of inertia reduction in the inertial and primary frequency response of the system.
- A line-to-line fault at B1 cleared after 41.5 ms (which is about 2.5 cycles). This type of fault was selected partly because it was the most common during the Blue Cut fire event [20]. This is an event for which a SI controller must not negatively respond and for which these type of controllers are rarely designed (as the design is based on the emulation of the inertial response of a synchronous generator). However, if a SI control is enabled it is important to verify that in fact the controller is harmless in all situations.
- A line-to-line fault at B1 cleared after 41.5 ms (which is about 2.5 cycles). This type of fault was also present during the Blue Cut fire event [20].

Fig. 16 shows the frequency of the system for the different CIG integration and control cases considered for the load connection event. To focus on the inertial response of the system, the figure show results only for the first 2 seconds following the disturbance. The results in Fig. 16 show that the controller has its intended effect and reduces the ROCOF of the system following the event. In fact, in cases where the control is included there is an improvement in the ROCOF with respect to the base case. Fig. 17 shows the power (without the scheduled value) injection of either the conventional generator or the CIG at Bus BG1 after the event. This figure shows that in the case, immediately after the load is connected, the conventional generator injects power which briefly and slightly goes up before slowly decaying. In contrast, for the SI control cases the power injection is slow but eventually surpasses that of the conventional generator. The case with the corrector is not different from the case without it because the corrector is never enabled as the IRM for this event is always below the threshold value, ϵ, of the frequency corrector. This latter fact can be observed in Fig. 18 and is explained because, as seen in Fig. 19, the load connection does not significantly distort the voltage waveform at BG1.

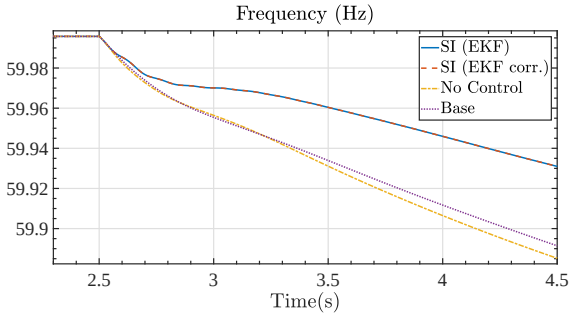

FIGURE 16. Frequency of the system following a 150 MW load connection at B1 in the system of Fig. 14.

This article has been accepted for publication in a future issue of this journal, but has not been fully edited. Content may change prior to final publication. Citation information: DOI 10.1109/ACCESS.2020.3044583, IEEE Access

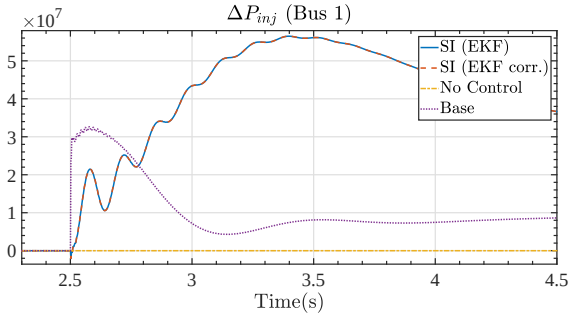

FIGURE 17. Power injection at Bus BG1 following a 150 MW load connection at B1 in the system of Fig. 14.

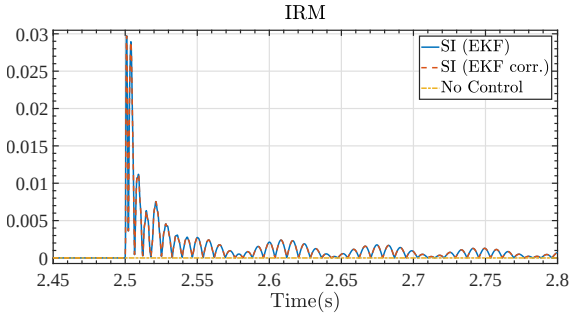

FIGURE 18. IRM of the EKF when estimating frequency out of voltage measurements for the load connection event.

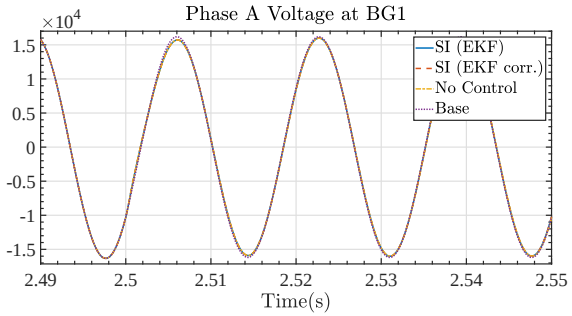

FIGURE 19. Voltage of phase at Bus BG1 following the load connection event.

Fig. 20 shows the frequency of the system for the SI control cases considered for the line-to-line event. For the base case this figure shows that the event causes the frequency to initially increase up to a value of 60.04 Hz (110 ms after the fault) and then slowly decrease to reach a value close to the nominal. For the case of CIG integration with no control the response is similar but faster. For the case of SI control without the frequency correction algorithm enabled, the results show that the system loses synchronism; in fact G2 separates from the system. Recall that this is the same controller that in Fig. 16 is shown to provide a beneficial support to the frequency regulation of the system. The results show that when the frequency corrector algorithm is included the response of the system is very similar to the one with no control as the action of the frequency corrector was rightfully triggered after the event. This is because, as observed in Fig. 22, the EKF IRM goes above the frequency

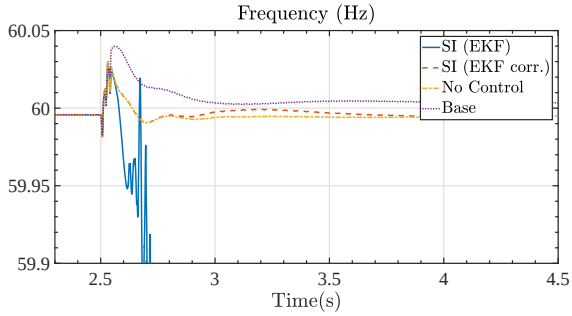

FIGURE 20. Frequency of the system following a line-to-ground event at B1 for the system shown in Fig. 14.

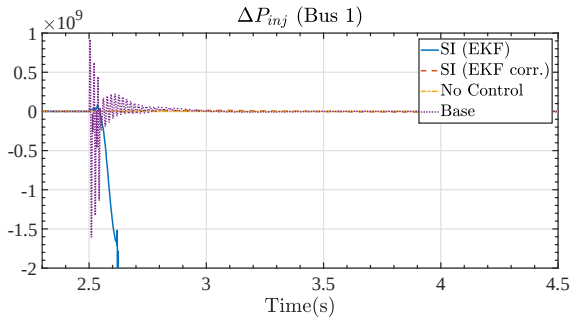

FIGURE 21. Power injection at Bus BG1 following the line-to-ground event at B1.

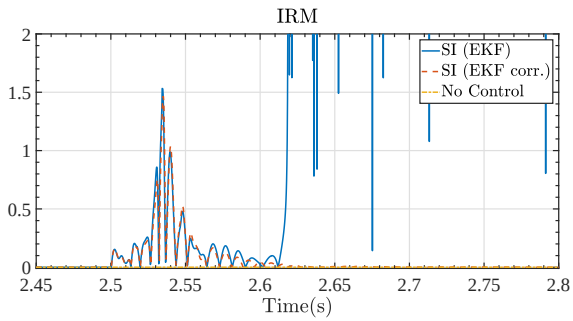

FIGURE 22. IRM of the EKF when estimating frequency out of voltage measurements line-to-ground event at bus B1.

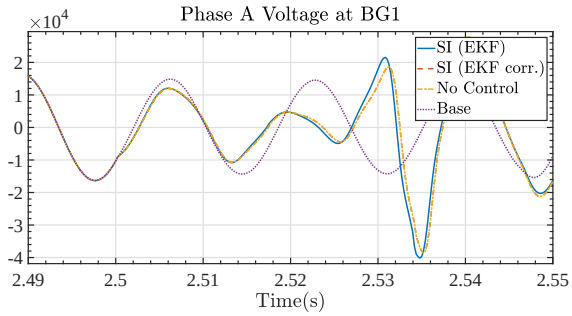

FIGURE 23. Voltage of phase at Bus BG1 following the line-to-ground event at bus B1.

corrector threshold (ϵ) following the fault inception. Fig. 21 shows the power modulation of the actuator for the line-to-line disturbance. This figure shows that the response of a

This article has been accepted for publication in a future issue of this journal, but has not been fully edited. Content may change prior to final publication. Citation information: DOI 10.1109/ACCESS.2020.3044583, IEEE Access

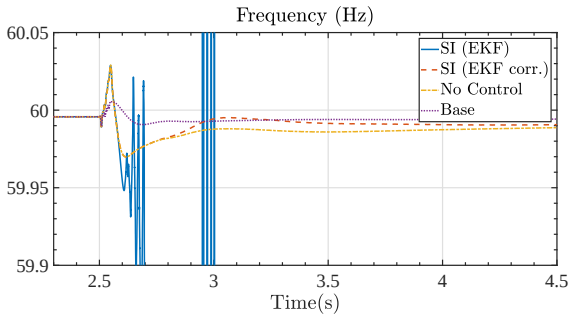

FIGURE 24. Frequency of the system following a line-to-line event at B1 for the system shown in Fig. 14.

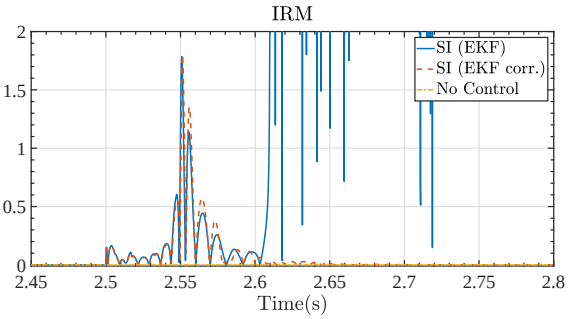

FIGURE 26. IRM of the EKF when estimating frequency out of voltage measurements line-to-line event at bus B1.

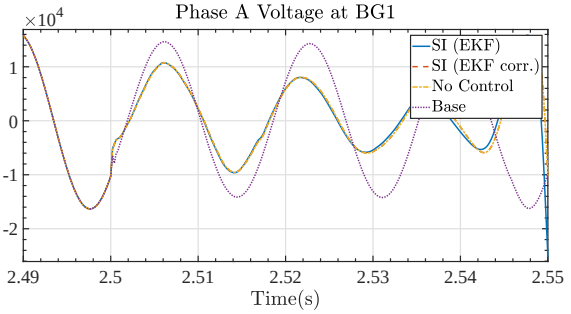

FIGURE 27. Voltage of phase at Bus BG1 following the line-to-line event at bus B1.

conventional generator is oscillatory while the responses of the CIG are not. The response of the case where there is no corrector stage becomes negative not too long after the fault which exacerbates its effect and is what ultimately causes the system break out. The results in Fig. 20 show that the proposed frequency corrector is crucial to block incorrect actions by the SI controller due to faulty frequency estimates. The corrector action lasts for about 200 ms after the event and the ramp rate stage was necessary to avoid steps in the estimated frequency (f_k^{corr}). These steps are to be avoided because when differentiated cause spikes in the CIG power injection which in turn distort the voltage waveform to the point where the corrector action may be again triggered. Fig. 23 presents the phase A voltage waveform at the beginning of the line-to-line event. These waveforms show that the signal is severely distorted for the cases of CIG integration.

Fig. 24 shows the frequency of the system for the SI control cases considered for the line-to-ground event. The results show a similar behavior to those in Fig. 20: the system loses synchronism for the case where the SI controller does not have the frequency corrector but is able to remain stable when the corrector is included. The results in Figs. 25, 26, and 27 are akin to those in Figs. 21, 22, and 23 and show that the faulty power injection by the CIG due to an incorrect frequency estimate is the main contributor to the loss of synchronism .

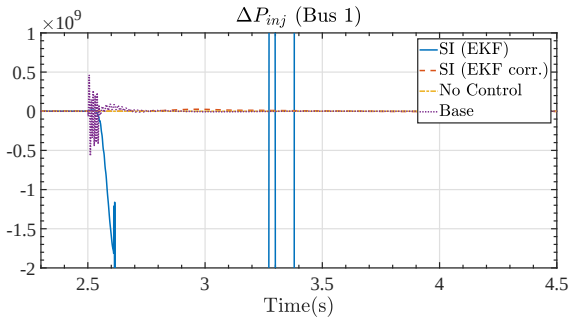

FIGURE 25. Power injection at Bus BG1 following the line-to-line event at B1.

The results in Figs. 20 and 24 convey an important message: control strategies aimed at enhancing the inertial and primary frequency regulation of the system can have unintended consequences for disturbances for which they were not specifically designed. And some of these consequences can only be analyzed in electromagnetic transient simulation platforms that are able to reproduce actual waveforms and distortions that a power system can exhibit and that are not possible to represent adequately with positive sequence simulation software. The authors understand that many challenges arise when considering the advocated approach for large scale power systems; this paper aims only at fostering the discussion on how to approach the coming challenges for a grid with more power electronics based generation.

V. CONCLUSION

This paper presents three three frequency estimation algorithms: EKF, QPLL, and ANF. The paper shows how internal signals of these algorithms can be used as metrics for frequency estimate reliability. The paper shows that these IRMs work even for signals contaminated with noise. The paper then proposes a frequency corrector algorithm to improve the estimates of the presented algorithms. This corrector is based on the IRM and is tested with signals with phase-steps and with severe distortions caused by line-to-line faults.

The paper tests the frequency corrector in a SI application where this controller is driven by the corrected frequency estimate. The SI control is included to a CIG in a test power system. The paper shows that the frequency corrector: (i) allows the SI action to enhance the inertial response of the system when the power quality of the signal is appropriate; and (ii) prevents the SI controller from performing unde-

sirable actions with negative impact to the system in cases where this type of control action is seldom tested.

Future avenues of research will include scaling up the test system and including a higher fidelity model for the converter of the CIG.

ACKNOWLEDGMENT

Sandia National Laboratories is a multimission laboratory managed and operated by National Technology and Engineering Solutions of Sandia, LLC., a wholly owned subsidiary of Honeywell International, Inc., for the U.S. Department of Energy's National Nuclear Security Administration under contract DE-NA0003525.

This research was supported by the U.S. Department of Energy Advanced Grid Modeling program. The views expressed in the article do not necessarily represent the views of the U.S. Department of Energy or the United States Government.

The authors of this paper would like to thank Mr. Ricky Concepcion for implementing the initial version of the frequency estimation algorithms used in this paper.

REFERENCES

[1] A. Mullane and M. O'Malley, "Modifying the inertial response of power-converter based wind turbine generators," in *The 3rd IET Int. Conf. on Power Electronics, Machines and Drives*, Dublin, Ireland, 2006, pp. 121–126.

[2] F. Wilches-Bernal, J. H. Chow, and J. J. Sanchez-Gasca, "A fundamental study of applying wind turbines for power system frequency control," *IEEE Transactions on Power Systems*, vol. 31, no. 2, pp. 1496–1505, 2015.

[3] R. Eriksson, N. Modig, and K. Elkington, "Synthetic inertia versus fast frequency response: a definition," *IET Renewable Power Generation*, vol. 12, no. 5, pp. 507–514, 2017.

[4] R. J. Concepcion, F. Wilches-Bernal, and R. H. Byrne, "Effects of communication latency and availability on synthetic inertia," in *2017 IEEE Power & Energy Society Innovative Smart Grid Technologies Conference (ISGT)*. IEEE, 2017, pp. 1–5.

[5] D. Belega and D. Petri, "Accuracy analysis of the multicycle synchrophasor estimator provided by the interpolated dft algorithm," *IEEE Transactions on Instrumentation and Measurement*, vol. 62, no. 5, pp. 942–953, 2013.

[6] P. Romano and M. Paolone, "Enhanced interpolated-dft for synchrophasor estimation in fpgas: Theory, implementation, and validation of a pmu prototype," *IEEE Transactions on Instrumentation and Measurement*, vol. 63, no. 12, pp. 2824–2836, 2014.

[7] A. G. Phadke and J. S. Thorp, *Synchronized phasor measurements and their applications*. Springer, 2008, vol. 1.

[8] "IEEE/IEC International Standard - Measuring relays and protection equipment - Part 118-1: Synchrophasor for power systems - Measurements," *60255-118-1-2018*, vol. 1.0, pp. 1 –78, 2018-12.

[9] S. Golestan, M. Ramezani, J. M. Guerrero, F. D. Freijedo, and M. Monfared, "Moving average filter based phase-locked loops: Performance analysis and design guidelines," *IEEE Transactions on Power Electronics*, vol. 29, no. 6, pp. 2750–2763, 2013.

[10] F. Wilches-Bernal, J. Wold, R. Concepcion, and J. Budai, "A method for correcting frequency and RoCoF estimates of power system signals with phase steps," in *51st North American Power Symposium (NAPS)*. IEEE, 2019, pp. 1–5.

[11] P. Dash, A. Pradhan, and G. Panda, "Frequency estimation of distorted power system signals using extended complex kalman filter," *IEEE Transactions on Power Delivery*, vol. 14, no. 3, pp. 761–766, 1999.

[12] K. Nishiyama, "A nonlinear filter for estimating a sinusoidal signal and its parameters in white noise: On the case of a single sinusoid," *IEEE Transactions on Signal Processing*, vol. 45, no. 4, pp. 970–981, 1997.

[13] H. Sahoo, P. Dash, and N. Rath, "Frequency estimation of distorted non-stationary signals using complex h_∞ filter," *AEU-International Journal of Electronics and Communications*, vol. 66, no. 4, pp. 267–274, 2012.

[14] K. Nishiyama, "Robust estimation of a single complex sinusoid in white noise-h/sub/spl infin//filtering approach," *IEEE Transactions on Signal Processing*, vol. 47, no. 10, pp. 2853–2856, 1999.

[15] R. Chudamani, K. Vasudevan, and C. Ramalingam, "Real-time estimation of power system frequency using nonlinear least squares," *IEEE Transactions on Power Delivery*, vol. 24, no. 3, pp. 1021–1028, 2009.

[16] M. Mojiri, M. Karimi-Ghartemani, and A. Bakhshai, "Estimation of power system frequency using an adaptive notch filter," *IEEE Transactions on Instrumentation and Measurement*, vol. 56, no. 6, pp. 2470–2477, 2007.

[17] D. Yazdani, A. Bakhshai, G. Joos, and M. Mojiri, "A nonlinear adaptive synchronization techniquefor grid-connected distributed energy sources," *IEEE Transactions on power electronics*, vol. 23, no. 4, pp. 2181–2186, 2008.

[18] L. Hsu, R. Ortega, and G. Damm, "A globally convergent frequency estimator," *IEEE Transactions on Automatic Control*, vol. 44, no. 4, pp. 698–713, 1999.

[19] P. S. Wright, P. N. Davis, K. Johnstone, G. Rietveld, and A. J. Roscoe, "Field measurement of frequency and rocof in the presence of phase steps," *IEEE Transactions on Instrumentation and Measurement*, 2018.

[20] "1,200 MW fault induced solar photovoltaic resource interruption disturbance report – Southern California 8/16/2016," North American Electric Reliability Corporation (NERC), Altanta, GA, Tech. Rep. Version 1.1, June 2017.

[21] L. Zhan, B. Xiao, F. Li, H. Yin, W. Yao, Z. Li, and Y. Liu, "Fault-tolerant grid frequency measurement algorithm during transients," *IET Energy Systems Integration*, vol. 2, no. 3, pp. 173–178, 2020.

[22] R. E. Kalman, "A new approach to linear filtering and prediction problems," *Transactions of the ASME–Journal of Basic Engineering*, vol. 82, no. D, pp. 35–45, 1960.

[23] H. Karimi, M. Karimi-Ghartemani, and M. R. Iravani, "Estimation of frequency and its rate of change for applications in power systems," *IEEE Transactions on Power Delivery*, vol. 19, no. 2, pp. 472–480, 2004.

[24] A. Riepnieks and H. Kirkham, "An introduction to goodness of fit for pmu parameter estimation," *IEEE Transactions on Power Delivery*, vol. 32, no. 5, pp. 2238–2245, 2016.

[25] M. Klein, G. J. Rogers, and P. Kundur, "A fundamental study of inter-area oscillations in power systems," *IEEE Trans. Power Syst.*, vol. 6, no. 3, pp. 914–921, Aug. 1991.

[26] W. H. Balliet, F. Wilches-Bernal, and J. Wold, "A testbed for synthetic inertia control design using point-on-wave frequency estimates," in *2020 IEEE Power & Energy Society General Meeting*. IEEE, 2020, pp. 1–5.

FELIPE WILCHES-BERNAL (S'12–M'16–SM'20) received the M.S. degree in control systems and signal processing from Université Paris-Sud XI, Orsay, France and the Ph.D. degree in electrical engineering from Rensselaer Polytechnic Institute, Troy, NY, USA. He joined the Electric Power Systems Research Department at Sandia National Laboratories, Albuquerque, NM, USA in 2015 where he currently works as a Senior Member of Technical Staff. Since joining in Sandia, he has served as a key technical contributor and PI/Co-PI of multiple projects in the power systems integration area. His research experience and interests include power system stability and control, renewable energy and smart grid technologies, and signal processing and control techniques applied to power systems. He was a key contributor of the team that was awarded the 2017 R&D 100 award for developing a control system for active damping of inter-area oscillations.

JOSH WOLD (S'12-M'16) received his B.S. in Electrical Engineering from Montana Tech in 2009. He joined Montana Tech's faculty in 2013 and received his PhD in 2015. He is now an Associate Professor of Electrical Engineering. His research interests include signal processing and controls applied to power systems.

W. HILL BALLIET is an ORISE science, technology, and policy fellow supporting the DOE's Water Power Technologies Office and their HydroWIRES initiative. His research interests are in grid dynamics, resource adequacy, and renewable energy integration. He earned a B.S. in general engineering from Harvey Mudd College and an M.S. in electrical engineering from the University of Southern California, where he focused on power systems and controls. During his master's, he interned at Sandia National Laboratories, where he worked on a simulation testbed for synthetic inertia using point-on-wave frequency estimates.